Role of the *S. typhimurium* Actin-Binding Protein SipA in Bacterial Internalization

Daoguo Zhou,[1] Mark S. Mooseker,[2] Jorge E. Galán[1]*

Entry of the bacterium *Salmonella typhimurium* into host cells requires membrane ruffling and rearrangement of the actin cytoskeleton. Here, it is shown that the bacterial protein SipA plays a critical role in this process. SipA binds directly to actin, decreases its critical concentration, and inhibits depolymerization of actin filaments. These activities result in the spatial localization and more pronounced outward extension of the *Salmonella*-induced membrane ruffles, thereby facilitating bacterial uptake.

Entry of *Salmonella typhimurium* into host cells requires a bacterially encoded type III protein secretion system (*1*). Upon its activation after bacterial contact with the host, this system delivers several bacterial proteins into the host cell cytosol (*2*). These effector proteins trigger host cell signaling pathways that lead to profuse actin cytoskeleton rearrangements and membrane ruffling, ultimately resulting in bacterial internalization (*3*). One such protein is SopE (*4, 5*), which activates small guanosine triphosphatases (GTPases) of the Rho subfamily such as CDC42 and Rac-1.

In a search for other bacterial effectors, we focused on SipA (*6*), a substrate of the type III secretion system that shares amino acid sequence similarity to IpaA, a *Shigella* spp. protein that is necessary for efficient bacterial entry into epithelial cells (*7*). We examined the interaction of a *S. typhimurium sipA* null mutant strain with cultured HeLa epithelial cells using an assay that allows the examination of both actin cytoskeleton reorganization and bacterial internalization after short infection times (*8*). The mutant was less effective than the wild-type strain in inducing actin cytoskeletal reorganization, and the rearrangements were diffuse rather than localized (Fig. 1, A and B). In addition, the internalized mutant bacteria appeared to be evenly distributed within the infected cell, whereas the wild-type strain was localized in clusters. A plasmid encoding SipA rescued the mutant phenotype (Fig. 1C). The *sipA* mutant was also impaired in its ability to be internalized by cultured epithelial cells after short infection times (Table 1). Over time, the defect in internalization was reduced, and beyond 30 min of infection there was almost no measurable difference between the entry levels of the wild type and the *sipA* mutant (Table 1). These results indicate that SipA is involved in the induction of localized actin cytoskeleton rearrangements and is required for efficient *S. typhimurium* entry into cultured epithelial cells.

To search for cellular proteins that interact with SipA, we used a glutathione S-transferase (GST) pull-down assay (*9*). HeLa cell lysates were incubated with GST-SipA or GST alone that had been immobilized on glutathione-agarose beads. The major GST-SipA–binding protein was actin (Fig. 2, A and B). The interaction of these proteins was shown to be direct (Fig. 2C) and was confirmed in a yeast two-hybrid assay (*10*). To examine whether the SipA-actin complex forms as a result of bacterial infection, we infected HeLa cells with wild-type *S. typhimurium* or an isogenic *sipA* mutant and looked for the complex by coimmunoprecipitation analysis (*11*). Actin was readily detected in SipA immunoprecipitates from cells infected with wild-type bacteria, but not in those from uninfected cells or cells infected with the *sipA* mutant (Fig. 2D).

To study the actin-binding activity of SipA in more detail, we carried out a cosedimentation assay (*12*). Constant amounts of filamentous (F) actin, which is composed of polymerized actin monomers (G-actin), were mixed with variable amounts of purified SipA before centrifugation, and the amount of SipA cosedimented with F-actin in the pellet was quantitated by densitometric analysis of Coomassie blue–stained gels. Under these experimental conditions, the binding of SipA to F-actin was saturable and the stoichi-

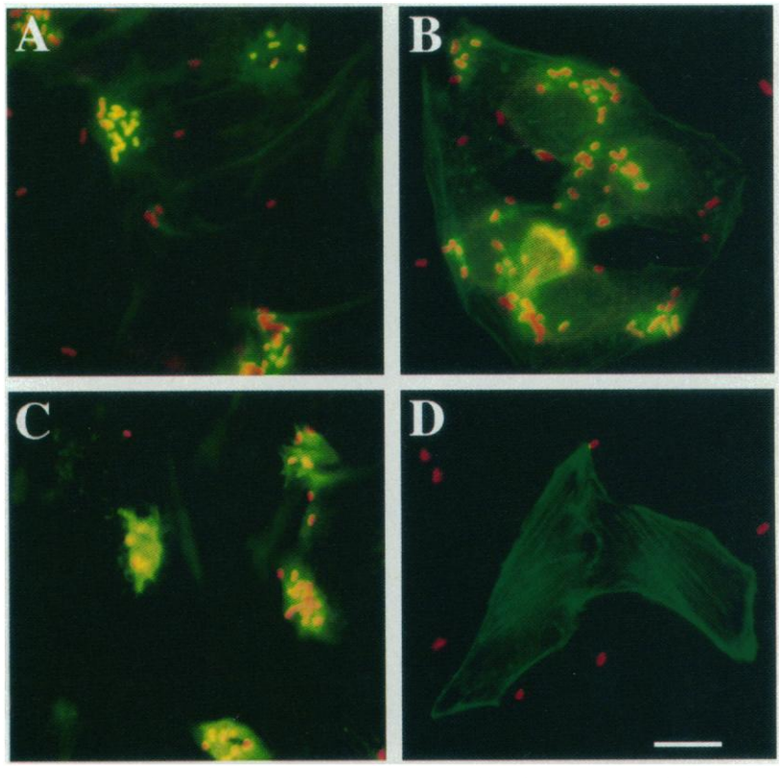

Fig. 1. Requirement of SipA for *S. typhimurium* induction of localized actin cytoskeleton rearrangements in HeLa cells. Cells were infected with wild-type *S. typhimurium* (**A**), the *sipA* mutant (**B**), the *sipA* mutant complemented with p*sipA* (a plasmid carrying *sipA*) (**C**), or the invasion-deficient *invA* mutant (**D**). The actin cytoskeleton was visualized by phalloidin staining (green), which stains F-actin. Bacteria (red) were stained with a polyclonal antibody to the *S. typhimurium* O-antigen (Difco, Detroit). Images were captured with a Hamamatsu C2400 charge-coupled device camera and pseudocolored. Exposure times for all the images are the same. Scale bar, 20 μm.

[1]Section of Microbial Pathogenesis, Boyer Center for Molecular Medicine, Yale School of Medicine, New Haven, CT 06536, USA. [2]Department of Molecular, Cellular and Developmental Biology, Yale University, New Haven, CT 06511, USA.

*To whom correspondence should be addressed. E-mail: jorge.galan@yale.edu

ometry of SipA to actin was approximately 1:1, suggesting that there is only one actin-binding site per SipA molecule (Fig. 3A). We also examined the actin-SipA complex by electron microscopy (*13*). The SipA-actin filaments were slightly larger in diameter than the actin filaments alone (actin, 6.5 ± 0.8 nm; actin plus SipA, 7.2 ± 0.7 nm). They were straighter, and they showed less obvious helical twist and subunit structure along the filaments (Fig. 3B).

We investigated the effect of SipA on actin dynamics using a pyrene-actin assay (*14*). The fluorescence of pyrene-actin increases when it is incorporated into F-actin and therefore can be taken as a direct measure of actin polymerization. We first measured the concentration of G-actin required for polymerization (critical concentration) in the presence or absence of SipA. Addition of SipA significantly reduced the critical concentration of G-actin from ~0.25 μM to as low as 0.02 μM (Fig. 4A). Analogous results were obtained in experiments in which F-actin was diluted in the presence or absence of SipA (Fig. 4B). We also investigated the influence of SipA on the kinetics of actin polymerization. Pyrene–G-actin (1 μM) was incubated with SipA (1 μM) and the rate of polymerization was monitored over time by fluorescence intensity measurements. Addition of SipA did not alter the rate of actin polymerization (Fig. 4C), suggesting that this protein does not nucleate actin. There was a slight decrease in fluorescence intensity in the presence of SipA, but this was due to the quenching of pyrene-actin by SipA rather than an effect on actin polymerization. At saturating levels, SipA quenched 32 ± 0.2% of the pyrene–F-actin fluorescence (mean ± SD of three determinations).

We next examined the effect of SipA on F-actin depolymerization. Pyrene–F-actin (1 μM) in the presence or absence of SipA (1 μM) was diluted to 0.1 μM, and the fluorescence intensity was monitored over time. SipA greatly increased the stability of F-actin (Fig. 4D). In the presence of SipA, F-actin remained stable even after 60 min of incubation under conditions that, in the absence of SipA, resulted in almost complete depolymerization. The stabilizing effect of SipA was comparable to that of the fungal toxin phalloidin (Fig. 4D). Similar results were obtained when F-actin was diluted without KCl and $MgCl_2$, indicating that SipA also inhibits depolymerization induced by dilution into low ionic strength buffer (*15*). Incubation of F-actin with SopE, an unrelated *Salmonella* protein purified in an identical manner, did not increase F-actin stability (*15*). Electron microscopy confirmed these results: F-actin filaments were readily observable in the presence but not in the absence of SipA (*15*). The ability of SipA to inhibit actin depolymerization without affecting the rate of actin elongation excludes the possibility that the stabilizing effect is due to capping of the ends of the actin filaments.

Our results indicate that SipA is largely responsible for the spatial restriction of the cytoskeletal rearrangements that result from the activation of Rho GTPases during *S. typhimurium* infection. The related *Shigella* IpaA protein is involved in a similar phenotype, although it appears to exert its function by a completely different mechanism that involves binding vinculin (*7*). SipA does not bind vinculin (Fig. 2B), but rather it decreases the critical concentration of actin and it stabilizes actin filaments by inhibiting their depolymerization. This stabilizing function may promote outward extension of membrane ruffles and filopodia, thereby facilitating bacterial uptake. Thus, SipA may help to increase the net accumulation of actin filaments at the point of bacterial–host cell contact, or even to influence the position and polarity of these cross-linked filaments. Stabilizing the actin filaments at the bacterial-induced membrane ruffles may also facilitate

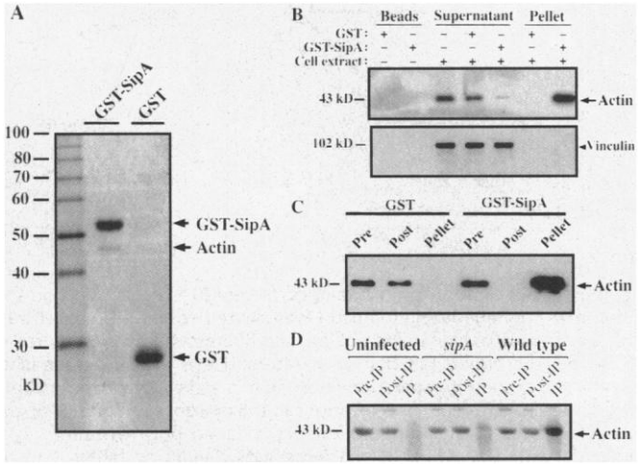

Fig. 2. Interaction of SipA with actin in vivo and in vitro. The interaction of SipA with F-actin in HeLa cell extracts was examined with a GST pull-down assay (*8*). Proteins bound to GST or GST-SipA beads were stained with Coomassie blue (**A**) or probed with an actin mAb (**B**, upper panel). As a control, the interaction of GST-SipA with vinculin was examined in a similar manner with an antibody to vinculin (B, lower panel). (**C**) The interaction of SipA with actin was also probed in extracts of *E. coli* expressing GST-SipA (*8*). The presence of F-actin bound to the GST-SipA (pellet) or the control GST beads, unbound in the cell extracts (post), or in the extracts before the reaction (pre) was detected on an immunoblot developed with an actin mAb. (**D**) The formation of the SipA-actin complex in infected HeLa cells was investigated by examining the proteins immunoprecipitated with an antibody to SipA (*10*). IP, immunoprecipitate. Left lane in (A) contains molecular size markers.

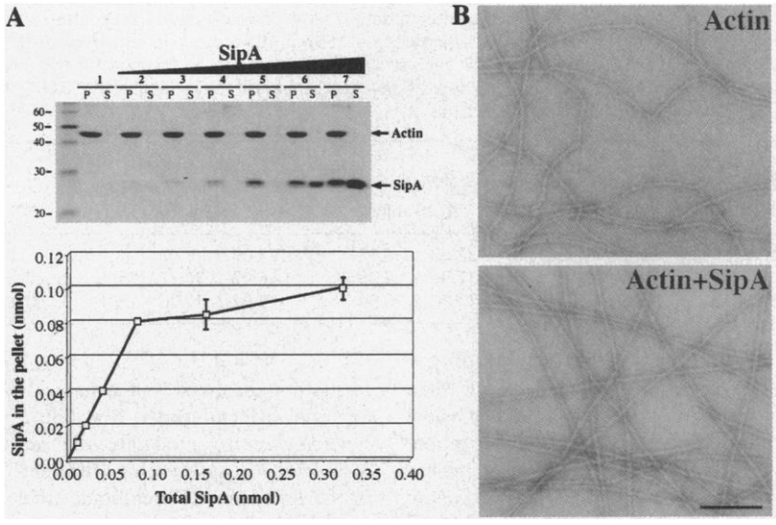

Fig. 3. Stoichiometry of the SipA-actin interaction. (**A**) The interaction of SipA and F-actin was examined by a cosedimentation assay (*11*). Coomassie blue–stained SDS gels of supernatants (S) and pellets (P) resulted from a 100,000*g* sedimentation of solutions containing varying amounts of SipA. The densitometric quantitation of SipA in the pellet is shown in the lower panel. (**B**) Electron micrographs of negatively stained F-actin (2 μM) incubated in the presence or absence of SipA (2 μM) (*13*). Scale bar, 0.1 μm.

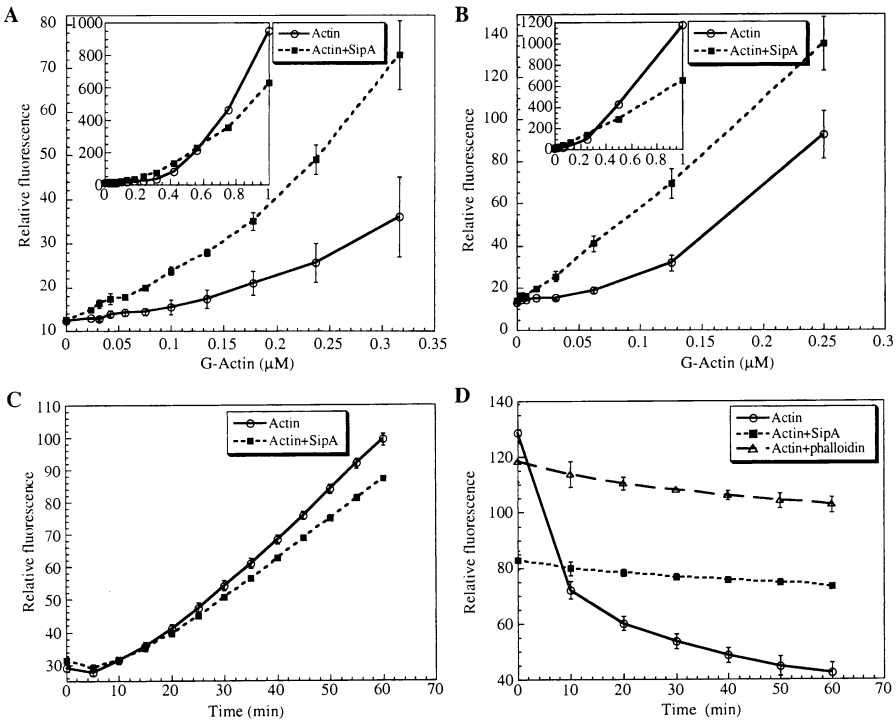

Fig. 4. Effect of SipA on actin dynamics. (**A** and **B**) Effect of SipA on the critical concentration of actin. In (A), pyrene-labeled G-actin was diluted to various concentrations in the presence and absence of equimolar amounts of SipA, and fluorescence was measured 4 hours after the initiation of the polymerization reaction (*14*). Alternatively, in (B), pyrene-labeled G-actin (4 μM) was polymerized at room temperature for 30 min in actin polymerization buffer. Polymerized actin was then diluted to different concentrations in the presence or absence of equimolar concentrations of SipA. (**C**) Effect of SipA on the kinetics of actin polymerization. Pyrene–G-actin (1 μM) was incubated with SipA (1 μM) in polymerization-inducing buffer, and fluorescence intensity was measured (*14*). (**D**) Effect of SipA on actin depolymerization. Pyrene–F-actin (1 μM) in the presence or absence of SipA (1 μM) or phalloidin (1 μM) was diluted to 0.1 μM in actin-polymerizing buffer, and the decrease in fluorescence intensity was followed over time. Bars represent SEs of three independent experiments.

Table 1. Requirement of SipA for efficient *S. typhimurium* entry into HeLa cells. Bacterial internalization was measured by fluorescence microscopy (*7*). Values are averages ± SE of three independent experiments and have been normalized to the internalization level of wild-type bacteria after 30 min of infection, which was considered to be 100% (in this case, 1597 ± 185 bacteria internalized per 100 cells). A minimum of 250 cells were counted for each strain per time point. The *P* values for the difference between the entry levels of the wild type and the *sipA* strains are as follows: 5 min, $P = 0.002$; 10 min, $P = 0.05$; 20 min, $P = 0.03$. IT, infection time.

Strain	Invasion (%)			
	IT 5 min	IT 10 min	IT 20 min	IT 30 min
Wild type	13.47 ± 1.93	32.68 ± 8.15	72.07 ± 9.43	100 ± 11.55
sipA	5.26 ± 0.99	17.91 ± 5.05	46.09 ± 10.77	92.27 ± 18.72
sipA/p*sipA*	11.29 ± 2.10	31.80 ± 10.98	71.92 ± 11.06	93.88 ± 11.10

the persistence of these filaments even when the concentration of G-actin has fallen below the critical concentration for polymerization.

Our results suggest a two-step mechanism for efficient entry of *S. typhimurium* into host cells. First, the bacterial protein SopE activates the small GTP-binding proteins CDC42 and Rac, components of the host signaling pathways that initiate actin cytoskeletal rearrangements and membrane ruffling. In a second step, these rearrangements are localized and enhanced by the bacterial effector SipA. The ability of *S. typhimurium* to modulate the actin cytoskeleton by influencing different stages in the formation of membrane ruffles is a remarkable example of pathogen evolution to modulate host cellular functions.

References and Notes

1. J. E. Galán, *Mol. Microbiol.* **20**, 263 (1996).
2. Y. Fu and J. E. Galán, *ibid.* **27**, 359 (1998); C. Collazo and J. E. Galán, *ibid.* **24**, 747 (1997); M. W. Wood, R. Rosqvist, P. B. Mullan, M. H. Edwards, E. E. Galyov, *ibid.* **22**, 327 (1996); E. E. Galyov *et al.*, *ibid.* **25**, 1903 (1997); W.-D. Hardt and J. E. Galán, *Proc. Natl. Acad. Sci. U.S.A.* **94**, 9887 (1997); W.-D. Hardt, H. Urlaub, J. E. Galán, *ibid.* **95**, 2574 (1998).
3. J. E. Galán and J. B. Bliska, *Annu. Rev. Cell Dev. Biol.* **12**, 221 (1996).
4. W.-D. Hardt, L.-M. Chen, K. E. Schuebel, X. R. Bustelo, J. E. Galán, *Cell* **93**, 815 (1998).
5. L. M. Chen, S. Hobbie, J. E. Galán, *Science* **274**, 2115 (1996).
6. K. Kaniga, D. Trollinger, J. E. Galán, *J. Bacteriol.* **177**, 7078 (1995); C. Collazo and J. E. Galán, *Infect. Immun.* **64**, 3524 (1996).
7. G. Tran Van Nhieu, A. Ben-Ze'ev, P. J. Sansonetti, *EMBO J.* **16**, 2717 (1997); G. Tran Van Nhieu and P. J. Sansonetti, *Curr. Opin. Microbiol.* **2**, 51 (1999).
8. The internalization into HeLa cells of wild-type *S. typhimurium* strain SL1344 [S. K. Hoiseth and B. A. Stocker, *Nature* **291**, 238 (1981)], the isogenic *sipA* mutant strain SB848, and its complemented derivative strain SB850 was measured by a fluorescence microscopy assay that can distinguish internalized from extracellular bacteria (*5*).
9. HeLa cells (~8×10^7) were harvested in 4.5 ml of phosphate-buffered saline (PBS) containing 0.1% NP-40 and 1 mM phenylmethylsulfonyl fluoride (PMSF) and disrupted with a glass grinder, and the cell lysates were cleared by centrifugation at 16,000*g* for 15 min. Alternatively, *E. coli* cells expressing GST-SipA were harvested in PBS containing 0.1% NP-40 and 1 mM PMSF and lysed by sonication. Total protein concentrations in the bacterial lysates were adjusted to ~2 mg/ml, and F-actin (Cytoskeleton Inc., Denver, CO) was added to a final concentration of 5 μg/ml. HeLa cell lysates (500 μl) were mixed with 10 to 20 μg of purified GST or GST-SipA bound to 50 μl of Sepharose beads, and the mixtures were incubated at 4°C for 4 hours (for most experiments, a fusion between GST and the COOH-terminal 226 amino acids of SipA was used). Samples were then centrifuged for 10 min at 1000*g* and supernatants were saved as postcapture samples. Beads were washed four times with ice-cold PBS containing 0.1% NP-40, resuspended in Laemmli sample buffer, and proteins separated on an 8% SDS-polyacrylamide gel. Proteins were stained, excised from the gel, and their mass determined by matrix-assisted laser desorption ionization mass spectrometry (MALDI-MS). Alternatively, interacting proteins were transferred to nitrocellulose membranes and probed with a mouse monoclonal antibody (mAb) to actin or vinculin (Sigma).
10. Introduction into the yeast indicator strain Y153 of a plasmid encoding a fusion of the last 226 amino acid residues of SipA to the Gal4 DNA-binding domain, along with a plasmid encoding full-length actin fused to the Gal4 activation domain, resulted in transformants that grew robustly in the absence of histidine and exhibited significant β-galactosidase activity (25.9 Miller units vs. 0.15 Miller units of the vector control).
11. HeLa cells seeded in 150-mm dishes were infected at a multiplicity of infection of 50 for 30 min. Cells were washed and then harvested into 2.5 ml of ice-cold PBS containing 0.1% NP-40 and 1 mM PMSF and disrupted with a glass grinder. SipA was immunoprecipitated with a mouse antibody to SipA from cell lysates that had been precleared for 2 hours at 4°C with normal mouse serum and protein A–Sepharose beads or GammaBind Plus Sepharose (Pharmacia). Immunocomplexes were recovered with protein A or GammaBind Plus Sepharose beads, and the presence of actin or vinculin was probed by immunoblotting with actin mAb (Sigma).
12. Actin binding was assayed by a cosedimentation assay [Y. Namba, M. Ito, Y. Zu, K. Shigesada, K. Maruyama, *J. Biochem.* **112**, 503 (1992)]. All samples were precleared by centrifugation at 100,000*g* for 30 min before use. G-Actin (Cytoskeleton Inc.) was polymerized in 50 mM sodium phosphate buffer (pH 7.0) containing 100 mM KCl, 0.1 mM adenosine triphosphate (ATP), 0.5 mM EGTA, and 1 mM $MgCl_2$ for 30 min at room temperature immediately before the binding assay and subsequently mixed with SipA. Mixtures (100 μl) were incubated at room tempera-

ture for 60 min and then centrifuged at 100,000*g* for 30 min at 4°C. Supernatants and pellets were analyzed by SDS–polyacrylamide gel electrophoresis (PAGE) and the relative amounts of the proteins in each fraction were estimated by scanning densitometry of the stained gels. In the absence of actin, no SipA (at all concentrations used in the assay) was detected in pellets after centrifugation at 100,000*g*.

13. Samples were loaded onto carbon-coated grids, stained with 1% uranyl acetate, and visualized under the electron microscope.
14. Actin was isolated was from rabbit skeletal muscle [J. A. Spudich and S. Watt, *J. Biol. Chem.* **246**, 4866 (1971)] and labeled with pyrene [T. Kouyama and K. Mihashi, *Eur. J. Biochem.* **114**, 33 (1981)]. Pyrene–G-actin (4 μM) was polymerized at room temperature for 30 min in actin polymerization buffer (APB) [20 mM Pipes (pH 7.0), 75 mM KCl, 2 mM $MgCl_2$, 0.1 mM EGTA, 0.1 mM dithiothreitol, and 0.05 mM ATP] and then diluted to different concentrations in the presence or absence of equimolar concentrations of SipA. After a 4-hour incubation at room temperature, the fluorescence intensity was measured on a fluorescence spectrophotometer (Hitachi F-2000) with excitation wavelength set at 365 nm and emission wavelength at 407 nm. Alternatively, pyrene–G-actin was diluted to various concentrations in the presence and absence of SipA in APB without KCl and $MgCl_2$. Polymerization was initiated by adding 75 mM KCl and 2 mM $MgCl_2$. After a 4-hour incubation at room temperature, the fluorescence intensity was measured as described above. To examine the effect of SipA on F-actin stability, we diluted 1 μM of polymerized actin, in the presence or absence of SipA (1 μM), in APB (with or without KCl and $MgCl_2$) to 0.1 μM and measured the fluorescence intensity over time. To evaluate the effect of SipA on actin polymerization, we precleared pyrene–G-actin by centrifugation at 100,000*g* for 4 hours at 4°C after dilution in APB without KCl and $MgCl_2$. Actin concentration was adjusted to 1 μM in the presence or absence of SipA (1 μM). Polymerization was initiated by adjusting the buffer concentration to 75 mM KCl and 2 mM $MgCl_2$, and the fluorescence intensity was measured over time.
15. D. Zhou and J. E. Galán, unpublished results.
16. We thank E. Taylor for providing pyrene-labeled actin, and members of the Galán laboratory for critical reading of the manuscript. Supported by NIH grants AI30492 and GM52543 (J.E.G.) and DK25387 (M.S.M.). J.E.G. is an investigator of the American Heart Association.

30 December 1998; accepted 2 March 1999

Regulation of Keystone Predation by Small Changes in Ocean Temperature

Eric Sanford

Key species interactions that are sensitive to temperature may act as leverage points through which small changes in climate could generate large changes in natural communities. Field and laboratory experiments showed that a slight decrease in water temperature dramatically reduced the effects of a keystone predator, the sea star *Pisaster ochraceus*, on its principal prey. Ongoing changes in patterns of cold water upwelling, associated with El Niño events and longer term geophysical changes, may thus have far-reaching impacts on the composition and diversity of these rocky intertidal communities.

It is predicted that increasing global temperatures will shift species' geographic ranges to higher latitudes or altitudes (*1*). On a local scale, communities may undergo gradual changes in composition as species with affinities for warmer temperatures become more abundant. However, temperature changes may have more immediate effects on local populations by altering the interaction between a species and its competitors, mutualists, predators, prey, or pathogens (*2*). Often a few key interactions contribute disproportionately to maintaining the composition and functioning of a community or ecosystem (*3*). If these interactions are sensitive to temperature, small climatic changes could generate system-wide ecological changes.

Here I report evidence from experiments in Oregon that slight fluctuations in water temperature regulate the impact of a keystone predator, the sea star *Pisaster ochraceus*, on its principal prey, the rocky intertidal mussels *Mytilus californianus* and *M. trossulus*. Paine's classic experiments in Washington state demonstrated that without predation on mussels by *Pisaster*, a diverse assemblage of low intertidal algae and invertebrates shifted to a monoculture of the competitively dominant mussel *M. californianus* (*4*). Densities of *Pisaster* and its effects on intertidal communities are highest during spring and summer in the Pacific Northwest (*5*, *6*). However, preliminary observations suggested that many sea stars became inactive in low zone channels or shallow subtidal waters during periods of upwelling (*6*). Water temperatures drop 3° to 5°C during these events, which generally last several days to three or more weeks (*7*). Upwelling is common along the Oregon coast from May to September.

I quantified sea star predation rates at three wave-exposed sites (*8*) within Neptune State Park (44°15′N, 124°07′W), Oregon, to test the hypothesis that the strength of the *Pisaster-Mytilus* interaction is reduced during periods of cold water upwelling. This 4-km stretch of coastline is composed of extensive rocky benches. The high intertidal zone is characterized by fucoid algae and barnacles, the mid zone by dense beds of *M. californianus*, and the low zone by a diverse mix of algae, sea grass, and invertebrates. At each site, I identified paired reefs (mean area ± SEM = 132.5 ± 49.7 m^2) isolated by surge channels. All sea stars were routinely removed from one reef in each pair and allowed to remain at natural densities on the other reef. In April and May 1997, I transplanted 20 clumps of 50 *M. californianus* (shell length, 4.5 to 5.5 cm) to the low intertidal zone on each reef (*9*).

From June through August 1997, I conducted five consecutive experiments to measure the intensity of sea star predation during periods lasting 14 days each. At the start of each period (*10*), I randomly selected and uncaged four mussel transplants per reef per site. I then recorded mussel survivorship and local sea star density (the number of sea stars in a 1-m radius around each transplant) on each of the first 6 or 7 days and again on day 14 (*11*). Temperature data-loggers installed in the low intertidal zone at each site recorded water temperatures when submerged, or air temperatures during low tide, every 30 min. Maximum air temperatures were used as a measure of potential heat stress during aerial exposure (*12*). Five maximum wave force dynamometers (*13*) at each site recorded variation in wave stress, a factor that can inhibit consumer activity.

The experiments encompassed periods with and without upwelling and thus tested whether per capita interaction strength [the difference in rates of mussel mortality on reefs with and without sea stars, divided by the local sea star density (*14*)] varied with fluctuations in water temperature. Per capita interaction strength was sharply reduced during a persistent upwelling event (Fig. 1, A and B). During upwelling, there was an even greater proportional drop in the collective impact of *Pisaster* (Fig. 1C) as a result of two effects: Individual sea stars consumed less (lower per capita effects), and the local density of sea stars was reduced (*15*), presumably as a result of more sea stars remaining inactive in channels or shallow subtidal waters. Both per capita and population interaction strength were significantly correlated with mean water temperature and were unrelated to variation in other environmental factors such as potential aerial heat stress or maximum wave forces (*16*).

I also examined *Pisaster* feeding rates in the laboratory (*17*) under three temperature regimes: constant 12°C, constant 9°C, and a

Department of Zoology, Oregon State University, Corvallis, OR 97331–2914, USA. E-mail: sanforde@bcc.orst.edu